PAPER

Non-contact magnetic actuated shape-programmable poly(aryl ether ketone)s and their structural variation during the deformation process

IOP Publishing Smart Materials and Structures
Smart Mater. Struct. **31** (2022) 035035 (12pp) https://doi.org/10.1088/1361-665X/ac4ff7

Non-contact magnetic actuated shape-programmable poly(aryl ether ketone)s and their structural variation during the deformation process

Shuai Yang[1], Yang He[1], Yanju Liu[2] and Jinsong Leng[1,*]

[1] Center for Composites Materials and Structures, Harbin Institute of Technology, Harbin, People's Republic of China
[2] Department of Astronautic Science and Mechanics, Harbin Institute of Technology, Harbin, People's Republic of China

E-mail: lengjs@hit.edu.cn

Received 13 September 2021, revised 27 January 2022
Accepted for publication 28 January 2022
Published 16 February 2022

Abstract

Here, a series of thermoplastic shape memory poly(aryl ether ketone)s (PAEKs) with programmable transition temperature were synthesized via a condensation polymerization reaction. The introduction of flexible segments and side groups onto PAEK main chains promoted the formation of the alternating rigid-flexible structures and the enhanced shape memory properties. The synthesized PAEKs exhibited the great thermal stability and strength which could greatly meet the demands in engineering applications. In addition, non-contact actuation of the shape memory behaviors of PAEKs was realized through the integration of Fe_3O_4 nanoparticles with magnetocaloric effect. More significantly, small-angle X-ray scattering analysis was utilized to reveal the transition of molecular chains and phase states during the stretching and heating processes. The change of internal structures and orientation of molecular chains during the deformation process might contribute to the regulation of shape memory behaviors. These studies on the fabrication of shape memory PAEKs with non-contact magnetic actuation performances and the investigation of their structural variation during the stretching and heating process were expected to open doors for the fabrication and investigation of new type of shape memory polymers.

Supplementary material for this article is available online

Keywords: shape memory PAEK, non-contact actuation, structural variation

(Some figures may appear in color only in the online journal)

1. Introduction

Shape-programmable polymers capable of reprogramming and revisable shape transformations, in responsive to the external stimuli, including heat [1], electric [2], light [3], and magnetic field [4], are highly desirable for a plethora of applications, including actuators, soft robots, biomedical devices, and aerospace structures [5–7]. Shape memory polymers (SMPs), as a kind of stimuli-responsive shape-programmable polymers, are able to memorize a temporary shape after deformation and recover the permanent shape in a predefined way [8–10], which attract the much attention and possess wide application prospect. Shape memory effect (SME) involves the

* Author to whom any correspondence should be addressed.

two characteristic steps. Step one is the programming step in which a structure is deformed from its permanent shape to a temporary shape, and step two is the recovery step where the original shape is recovered upon an appropriate stimulus [11, 12]. The shape maintaining and recovering functions for thermoplastic SMPs are mostly related to the freezing and melting of the long-range motion of chain segments at the different external temperatures (below and above the transition temperature of polymer network) [13–15]. Despite great efforts, to date there are several defects for SMPs, including poor mechanical performances, thermal properties, and low recovery force upon the external stimuli, which adverse to their applications [16, 17]. SMPs with excellent shape recovery ability are commonly found to possess undue toughness and poor stiffness. Therefore, one big challenge in such system is how to realize the synergistic effect of flexibility in shape recovery and strength in mechanical performances [18–20].

Poly(aryl ether ketone) (PAEK), a kind of high-performance engineering thermoplastics with the outstanding mechanical properties and thermal stability, has been attracting the great attention [21–23]. Besides, since the flexible molecular components of PAEK main chains and various side groups could be obtained through molecular chains designing [24], PAEK exhibits the excellent processability which possess plenty of applications, such as aerospace engineering, optical devices, and soft structures [25, 26]. It is meaningful to prepare PAEKs with the excellent SME and good mechanical properties via the introduction of flexible segments and groups, which would be conducive to the designing and manipulation of future engineering structures and devices based on PAEKs.

Typically, thermal-triggered SMPs involve transition temperature, such as glass transition temperature (T_g) or melting transformation temperature, to manipulate the shape fixity and recovery [27, 28]. Once external heating is impossible in application areas such as space, thermal-responsive SMPs could not be operated normally. Hence, researchers have attempted to develop the remote non-heating actuation methods for SMPs, such as light, microwave, magnetism, and so on [29–31]. Among these actuations, magnetic actuation could exploit wide applications due to the convenient manipulation and non-contact controllability [32–34]. Magnetic actuated systems normally utilize functional magnetic particles, such as Fe_3O_4 particles, to drive/control complex programmable shape deformation and recovery [35]. Upon magnetic field, these particles with programmed domains would exert micro-torques, resulting in the engendering of a large amount of heat, and leading to the macroscopic shape recovery [36].

In this paper, we proposed the fabrication of shape memory PAEKs with the enhanced mechanical strength and PAEK/Fe_3O_4 composite actuators with the non-contact actuated SME. Shape memory PAEKs were synthesized via the condensation polymerization, in addition that the strength, toughness, and shape memory behaviors were regulated via the tuning of flexible segments (carbon bonds, aryl carbonyl groups, and aryl ether groups). The SME of PAEKs could be modified via improving the flexibility of the backbones, and diverse switching temperatures of shape memory PAEKs were obtained through tuning the proportion of two bisophenol monomers. For the exploration of the internal structural transition of PAEK during the shape memory behaviors, we investigated the orientation of molecular chains during the heating and deformation processes via *in situ* small-angle X-ray scattering (SAXS) combined with heating and tensile modes. Besides, the incorporation of magnetic particles into SMP matrix was conducted to achieve non-contact magnetic-actuated SME. With the excellent strength and stability, the composite actuators that were non-contact magnetically actuated were able to fulfill the shape recovery process for various application opportunities.

2. Experimental

2.1. Materials

The 4,4′-(hexafluoroisopropylidene) diphenol, 2,2-bis (3-amino-4-hydroxyphenyl) hexafluoropropane, 4,4′-difluorobenzophenone, potassium carbonate (K_2CO_3), and tetramethylene sulfone (TMSF) were supplied by Aladdin Industrial. Toluene and N-methyl kelopyrrolidide (NMP) were all bought from Tianjin Guangfu Chemical Reagent Factory. Fe_3O_4 nanoparticles were bought from Macklin Reagent.

2.2. Synthesis of shape memory PAEKs

Shape memory PAEKs were synthesized via a condensation polymerization, as reported previously [37]. The 4, 4′-(hexafluoroisopropylidene) diphenol, 2,2-bis (3-amino-4-hydroxyphenyl) hexafluoropropane, 4,4′-difluorobenz ophenone, and K_2CO_3, according to a certain proportion, were added into a mixture of TMSF and toluene in a 100 ml three-neck flask equipped with Dean–Stark trap and nitrogen atmosphere. The temperature firstly increased to 140 °C for 2.5 h, to remove the moisture, followed by distilling the toluene and then heating to 170 °C for 3 h. Afterwards, the solid product was separated out via pouring the dense mixture into a beaker containing distilled water and isopropanol. Finally, the precipitate was filtered with deionized water and ethanol for several times, and dried at 40 °C for 24 h (yield: 94%). Synthesized PAEKs were signed to P1, P2, P3, P4, and P5, corresponding to the proportion of 2,2-bis (3-amino-4-hydroxyphenyl) hexafluoropropane and 4,4′-(hexafluoroisopropylidene) diphenol of 1:0, 0.75:0.25, 0.5:0.5, 0.25:0.75 and 0:1, respectively. The polymerization reaction is illustrated in scheme 1. In the main chains of synthesized PAEKs, the benzene rings were rigid segments, possessing stability of permanent shape and shape recovery capability. The carbon bonds, aryl carbonyl groups and aryl ether groups acted as flexible segments, responsible for the shape deformation and stability of temporary shape. The strongly polar amino groups adjusted the toughness of main chains. These alternating rigid-flexible regions endowed synthesized PAEKs the excellent shape memory behaviors.

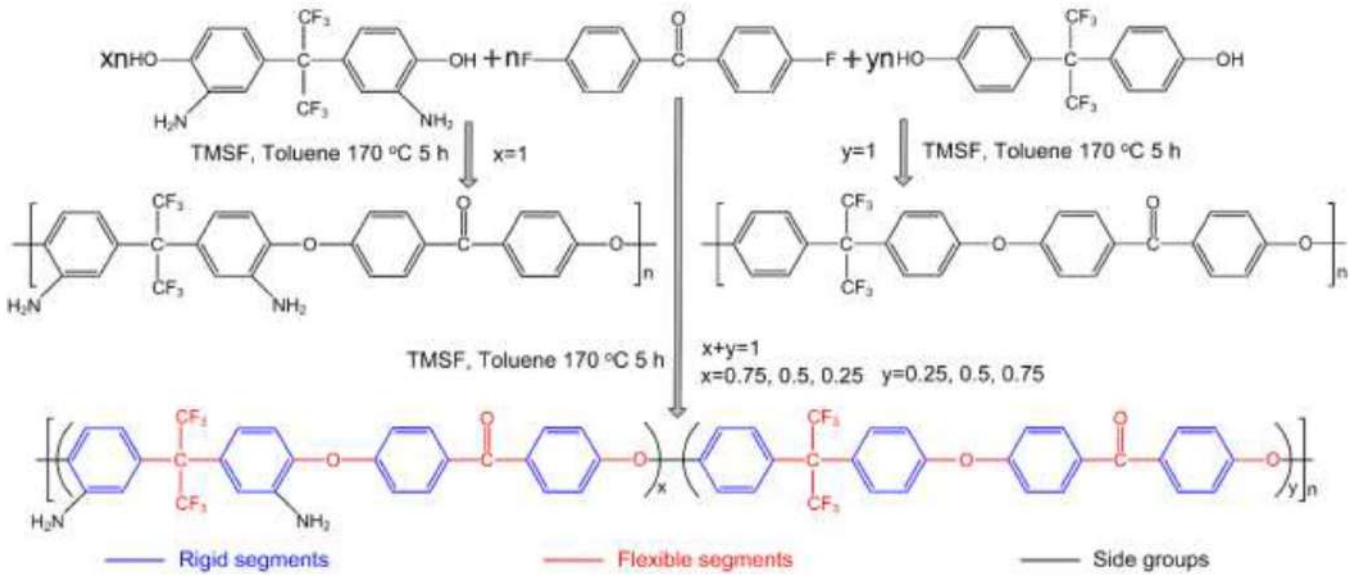

Scheme 1. Synthetic route of shape memory PAEKs.

2.3. Preparation of PAEK and PAEK/Fe_3O_4 composite films

A certain amount of prepared PAEKs were dissolved into NMP and stirred at 40 °C for 24 h. PAEK/Fe_3O_4 mixtures were obtained via blending P1 with a certain amount of Fe_3O_4 particles (0, 5, 10, 15, and 20 wt%). Mixtures were cast into a mold and dried at 80 °C for 48 h to obtain PAEK and PAEK/Fe_3O_4 composite films. Afterwards, the films were peeled off from the mold and stored carefully for measurements.

2.4. Characterization

^{1}H-nuclear magnetic resonance (^{1}H NMR) spectra was performed with an ADVANCE III 400 MHZ 010601 spectrometer (Bruker), in addition that using $CDCl_3$ as the solvent and tetramethylsilane as the internal reference. Fourier transform infrared (FTIR) spectroscopy was performed with a Spectrum Two (PerkinElmer). The spectral range was 4000–400 cm^{-1} with a resolution of 4 cm^{-1}.

Wide-angle X-ray diffraction (WAXD) patterns were obtained on an X'pert XRD analyzer (Panalytical B.V.), and a 2θ range of 5°–55° with a step size of 10° min^{-1}. SAXS spectra was collected through Shanghai Synchrotron Radiation Facility (BL19U2), and the obtained data were analyzed by RAW software. One-dimensional scattering profiles could be obtained by integrating the 2D patterns. The scattering vector (q) and the long period (L) of the samples were obtained as the equations:

$$q = \frac{4\pi \sin\theta}{\lambda}$$

$$L = \frac{2\pi}{q}$$

where q is the scattering vector, λ is the wavelength, and 2θ is the scattering angle. In addition, L is the long period of lamellar structures.

Differential scanning calorimetric (DSC) curves were obtained by a DSC 1 STAR System (Mettler-Toledo) at a temperature range of 25 °C–300 °C with a heating rate of 10 °C min^{-1}. Thermal gravimetric analysis (TGA) curves were performed on a TGA/DSC 1 STAR System (Mettler-Toledo) at a temperature range of 25 °C–800 °C, and a heating rate of 10 °C min^{-1}.

Static tensile tests were conducted with a loading rate of 4 mm min^{-1} by a universal mechanical testing machine (SBA-10, Hake Keji) at room temperature (about 25 °C). The specimens were cut to the sizes of 35 mm × 10 mm × 0.1 mm for testing. The testing results were averaged from five samples.

Dynamic mechanical analysis (DMA) curves were performed on a dynamic mechanical analyzer (Q800, TA Instruments) with a range of 25 °C–180 °C using a heating rate of 10 °C min^{-1}. The specimens were cut to the sizes of 30 mm × 3 mm × 0.1 mm.

2.5. Shape memory test

The heat-actuated shape memory behaviors were investigated via the 'U' shape film samples. The film samples were cut into a rectangle with sizes of 25 mm × 5 mm. Then, they were fixed into a 'U' shape above T_g. Afterwards, the heat source was removed, and the temporary shape was fixed at room temperature. The heating actuated SME was triggered by putting the sample on the heating plate with the constant temperature of T_g + 10 °C. The whole recovery process was recorded using a digital video camera, and the recovery ratio (R_r) and fixity ratio (R_f) were defined as follows:

$$R_r = \frac{\theta_{(t)} - \theta_0}{180 - \theta_0} \times 100$$

$$R_f = \frac{180 - \theta_0}{180} \times 100$$

where θ_0 is the deformation angle at the time of 0 s, and $\theta_{(t)}$ is the deformation angle at the time of t s.

The shape fixity of samples using in magnetic-actuated SME was the same mentioned above. The only difference was the triggering channel, and the magnetic-actuated recovery behaviors were triggered using an alternating magnetic field (27.9 kHz).

3. Results and discussion

3.1. Characterization

^{1}H NMR analysis was used to characterize the chemical structure of synthesized PAEKs, as shown in figure 1(a). For P1, the chemical shift at 1.53 ppm was concerned with the protons of amino groups on phenyl ring (5). Meanwhile, PAEK backbone was reflected through the protons of 1, 2, and 3, at 7.10, 7.28, and 7.81 ppm, respectively. For P2, P3, and P4, the chemical shifts of the protons of three were more significant, due to the increasing of 4,4′-(hexafluoroisopropylidene) diphenol. For P5, the chemical shift at 1.53 ppm disappeared, due to the abandoning of side amino groups. All the chemical shifts mentioned above indicated the formation of intrinsic structure of PAEKs.

Figure 1(b) shows FTIR spectra of the samples with various proportions of bisphenol monomer. The peaks at 3332 cm^{-1} was concerned with the characteristic peak of N–H bonds, which became moderate as the introduction of 4,4′-(hexafluoroisopropylidene) diphenol. The stretching vibration of aryl carbonyl groups was corresponding to the peak of 1585 cm^{-1}, and whose peak of symmetric stretching was at 930 cm^{-1} [38]. In addition, the peak at 1225 cm^{-1} was attributed to the characteristic peak of aryl ether groups.

WAXD curves are illustrated in figure 1(c). All the synthesized PAEKs showed semi-crystalline, and the diffraction peaks were at 2θ = 17.25°, 17.27°, 17.30°, 17.33°, and 17.38°, respectively. As the increasing of 4,4′-(hexafluoroisopropylidene) diphenol, the diffraction peak shifted slightly to higher degree.

DSC curves are showed in figure 1(d). It could be found that the glass transition temperature (T_g) of synthesized PAEKs increased gradually, through the increasing of 4,4′-(hexafluoroisopropylidene) diphenol. The corresponded T_g of P1, P2, P3, P4, and P5 was 121.9 °C, 124.2 °C, 127.1 °C, 130.6 °C, and 159.3 °C, respectively. Increasing the proportion of 4,4′-(hexafluoroisopropylidene) diphenol, side amino groups decreased, and as a result, the T_g increased.

Figure 1(e) shows their TGA curves. As the increasing of 4,4′-(hexafluoroisopropylidene) diphenol, the initial degradation temperature (T_i) increased (from 384.6 °C to 412.2 °C, 436.6 °C, 462.2 °C, and 488.9 °C, corresponding to P1, P2, P3, P4, and P5, respectively). This might be attributed to that the decreasing of side amino groups increased the thermal stability of whole molecular chains, hindering the degradation of polymer chains. Meanwhile, the temperature of maximum degradation rate (T_{max}) increased which was related to the same reason. In addition, as the increasing of thermal stability, the residual mass (ω_m) increased, while the temperature was up to 800 °C. The ω_m of P1, P2, P3, P4, and P5 was 49.2%, 51.2%, 52.4%, 52.9%, and 53.6%, respectively.

SAXS tests were used for further characterization of PAEKs. Two-dimensional SAXS patterns, 1D integral curves, and the long period and q_{max} statistical chart are showed in figure 2. In figure 2(a), all the synthesized PAEKs showed the similar diffuse scattering feature, which was circular and surrounded the beam spot. There were not any direct relations between different proportion of bisphenol monomers and the internal micro-structure. In figure 2(b), all the synthesized PAEKs showed the same q_{max}, which indicated that the internal micro-structure had no difference among the various proportions of synthesized PAEKs. According to Bragg's law, the long period (L) was calculated. The values that were not apparent different indicated the similar distribution of internal crystalline lamellae.

DMA curves are showed in figure 3. Figure 3(a) shows that the storage modulus of PAEKs increased gradually from P2 to P4, which was attributed to that the decreasing of side amino groups determined stability of molecular chains. As for P5, polymerized by the only bisphenol monomer of 4,4′-(hexafluoroisopropylidene) diphenol, the whole chains were of high regularity without side groups, exhibiting the highest storage modulus. Nevertheless, the modulus of P1 was not the lowest, between which of P3 and P4. It could be concerned with the decreased regularity of molecular chains of unitary repeating unit. Figure 3(b) shows that with the increasing of proportion of 4,4′-(hexafluoroisopropylidene) diphenol (from P1 to P5), the T_g almost increased gradually, in consistent with the results of DSC curves. Nevertheless, the T_g values were not the same, which could be concerned with the different testing mechanisms.

Static tensile test results of prepared PAEK films are showed in figure 4. The stress–strain curves in figure 4(a) illustrated that the fracture mode of P1, P2, P3, and P4 was brittle fracture. But for P5, which exhibited yield stage during the tensile process. As the increasing of 4,4′-(hexafluoroisopropylidene) diphenol, Young's modulus decreased gradually except for P5. In figure 4(b), the tensile strength of P1 was the highest, of 60.2 MPa. As the increasing of 4,4′-(hexafluoroisopropylidene) diphenol, the tensile strength decreased, of 46.43, 43.54, and, 31.08 MPa, corresponding to P2, P3, and P4, respectively. Due to the strong polarity, amino groups increased the stiffness of main chains, resulting in the enhanced strength. The tensile strength of P5 was 48.57 MPa, lower than that of P1. Comparing with other terpolymers (P2, P3, and P4), bipolymers (P1 and P5) possessed the relatively regular main chains, conducive to the mechanical performances. As shown in figure 4(d), the values of Young's modulus were 1.416, 1.014, 0.885, 0.609, and 1.201 GPa, corresponding to P1, P2, P3, P4, and P5, respectively. In figure 4(c), as the decreasing of side amino groups, the elongation at break of prepared samples increased gradually.

Figure 5 shows a set of digital images and SAXS patterns of P1 during the tensile test (horizontal tensile direction). The evolution of SAXS patterns could be concluded into four stages, as shown in figure 5(b). In stage I (before

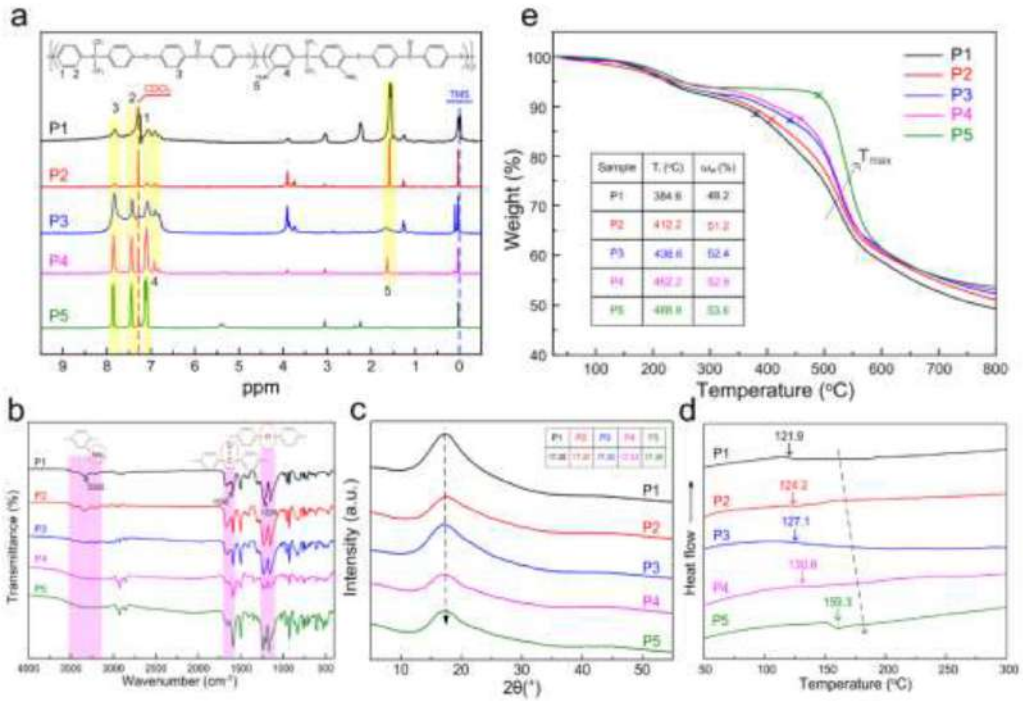

Figure 1. Characterization of synthesized PAEKs (P1, P2, P3, P4, and P5): (a) ^{1}H NMR spectra; (b) FTIR spectra; (c) WAXD curves; (d) DSC curves; (e) TGA curves.

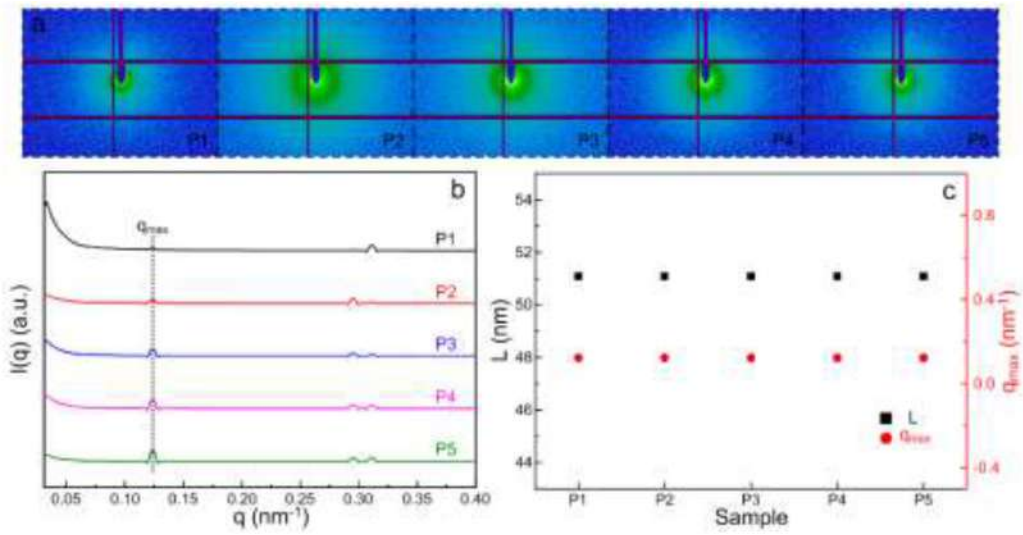

Figure 2. (a) Two-dimensional SAXS patterns; (b) 1D integral curves; (c) the long period and q_{max} as a function of prepared PAEKs.

the test, shown in figure 5(a) (I)), the sample showed the round scattered signals. Conducting the tensile process, the horizontal scattered fringes occurred (stage II), indicating the orientation of molecular chains in horizontal direction and the occurrence of microstacks in vertical direction, shown in figure 5(a) (II). With the continuing of constant-force stretching, the orientation of molecular chains and microstacks became clearer, and the scattered fringes became stronger. When the gathering of microcracks was so dense to destruct the whole construction of sample, the horizontal scattered fringes became weak, due to the vanishing of the most of microcracks, shown in figure 5(a) (IV). The scattered fringes were concerned with the orientation of molecular chains and the existence of microstacks occurred during the tensile process. In figure 5(c), the value of q_{max} decreased slightly during the tensile process. In addition, the long period increased, as shown in figure 5(d).

3.2. *Heat-actuated shape memory behaviors*

The heat-actuated SME of PAEKs films was characterized by the heat-actuated shape memory test, shown in figure 6. Figure 6(a) shows the whole shape recovery process of P1 film with the triggering temperature of 131 °C (T_g + 10 °C). The original shape of sample could be fully recovered in

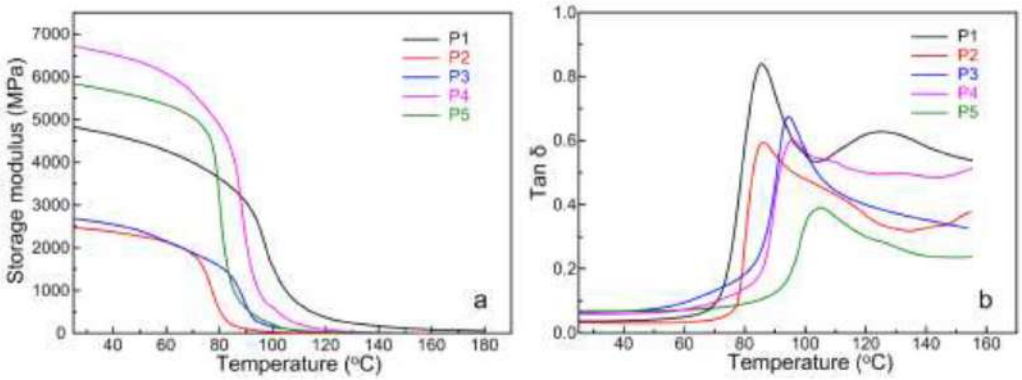

Figure 3. DMA patterns of prepared PAEKs (a) storage modulus; (b) tan δ.

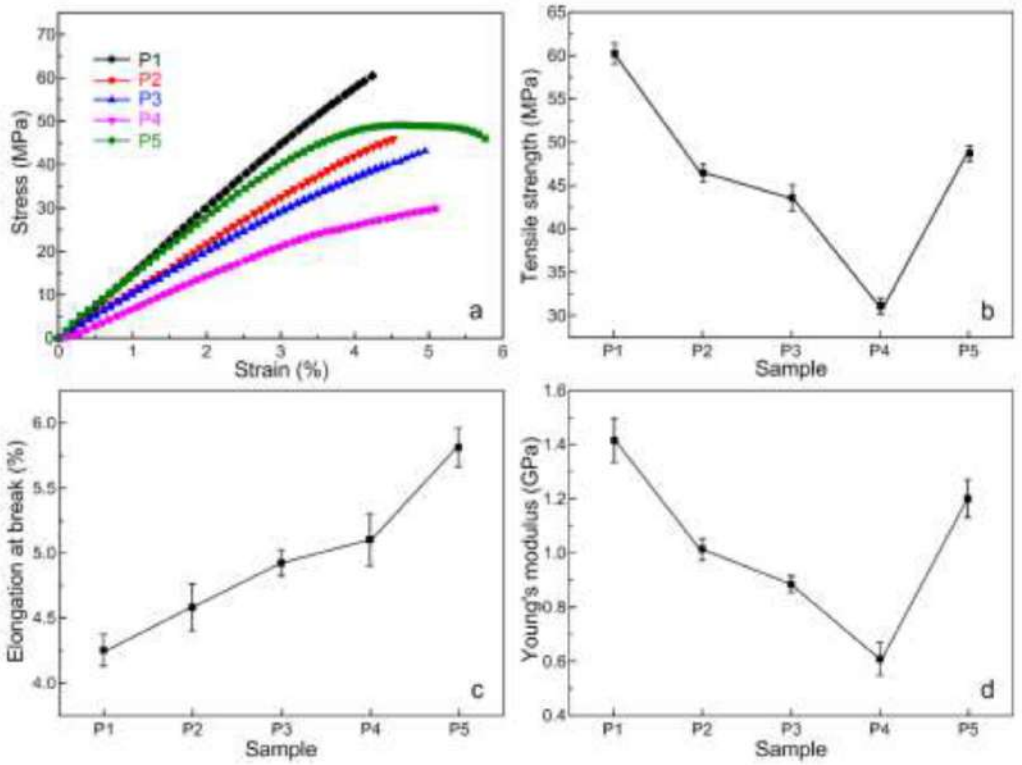

Figure 4. Static tensile test results of prepare PAEKs: (a) stress–strain curves; (b) tensile strength; (c) elongation at break; (d) Young's modulus.

macroscopic view, and the whole shape recovery process finished within 25 s, depicted in Video S1 (available online at stacks.iop.org/SMS/31/035035/mmedia). In figure 6(b), all the samples exhibited the excellent shape recovery ability, of R_r over 91%. With the decreasing of side amino groups, the recovery ratio increased gradually, from 91.6% to 92.7%, 95.1%, and 97.2%, corresponding to P2, P3, P4, and P5, respectively. As for P1, the recovery ratio was 95.5%, which could be attributed to the regularity of molecular chains, promoting the shape recovery. In figure 6(c), it could be obtained that the fixity ratio of all the samples was over 98%, indicating the excellent shape fixity. The little difference among the samples could be concerned with the regularity of main chains and the amount of side amino groups. Figure 6(d) shows the change trend of recovery ratio of P1 and P5 during the heating-actuated shape recovery process. It was obvious that the shape recovery process of P5 achieved faster, within 12 s, and the ultimate recovery ratio was 98.0%. The whole shape recovery process of P1 finished within 25 s, and the ultimate recovery ratio was 96.5%. At the initial stage of shape recovery process, the shape recovery of P1 was relatively slower. Nevertheless, P5 maintained the relatively uniform recovery pace during the recovery process. Figure 6(e) shows the recovery ratio of P1 and P5 after five times of consecutive shape recovery and refixation process. For P1, after five shape memory round processes, the recovery ratio decreased from 95.2% to 89.8%. For P5, the recovery ratio decreased from 97.2% to 92.1%. The recovery ratio of both two samples was stable in five consecutive cycles, indicating the great reproducibility of shape memory behaviors.

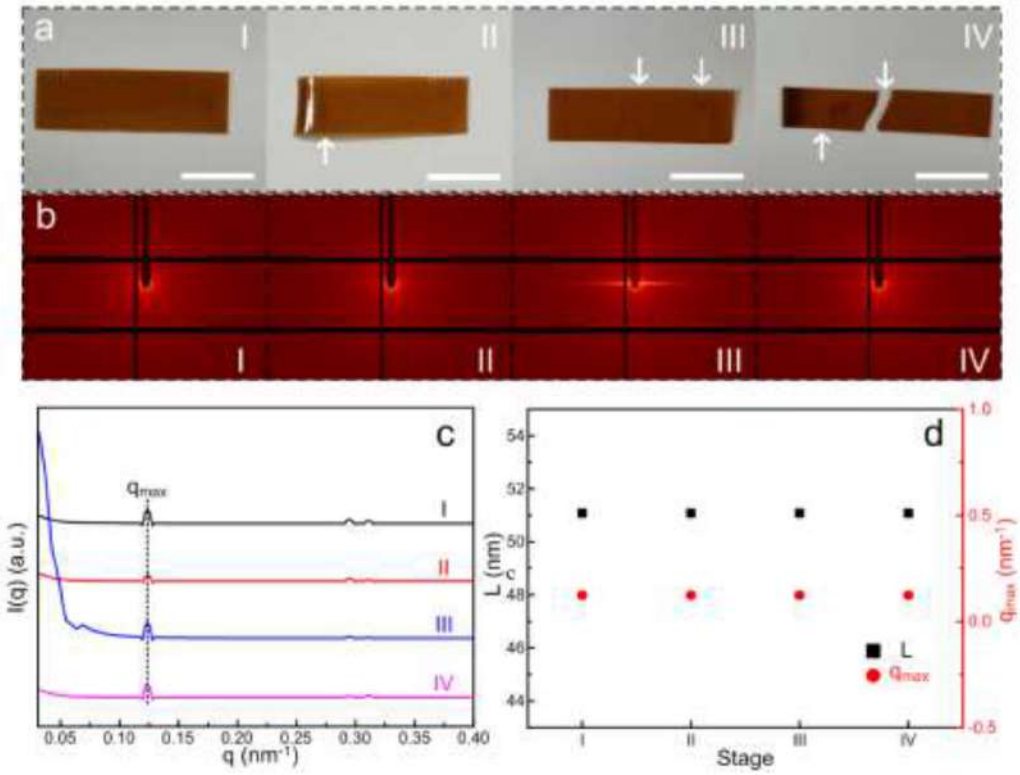

Figure 5. (a) Digital images and (b) 2D SAXS patterns; (c) 1D integral curves; and (d) the long period and q_{max} value of P1 during the tensile tests.

3.3. Non-contact magnetic-actuated shape memory behaviors

Non-contact magnetic-actuated shape memory behaviors of PAEK/Fe_3O_4 composite films were investigated through the corresponding magnetic-actuated shape memory test, depicted in figure 7. Figure 7(a) shows the whole shape recovery process of the composite film with Fe_3O_4 content of 15 wt%. The whole shape recovery process could be finished within 50 s, shown in Video S2. The temperature changes of the composite film during the recovery process were recorded by a thermal infrared imager, shown in figure 7(b). The heat dissipation rate of single film was too fast to heat the specimen above the temperature of T_g. Therefore, the magnetic-actuated composite film specimens were fabricated via the superposition of multiple films (four layers). The temperature monitor of thermal infrared imager was for the surface of specimen. Due to the heat dissipation, the surface temperature was relatively low, at around 60 °C during the recovery process. Meanwhile, the surface temperature of 60 °C indicated the necessary of superposition of multiple films. In figure 7(c), the composite film could not recover to the permanent shape when the Fe_3O_4 content was 5 wt%. As the increasing of Fe_3O_4 content, the recovery ratio increased gradually, of 76.5%, 88.9%, and 95.4%, corresponding to the Fe_3O_4 content of 10, 15, and 20 wt%, respectively. As the increasing of Fe_3O_4 content, the heat from magnetocaloric effect increased, elevating the temperature and as a result, the recovery ratio increased. Because the composite film with Fe_3O_4 content of 5 wt% could not achieve the shape recovery, the corresponding fixity ratio was not depicted in figure 7(d). All the samples exhibited the excellent fixity ratio over 99%, due to the intrinsic fixity ability of PAEK matrix and the incorporation of Fe_3O_4 particles. Figure 7(e) shows the recovery ratio of composite film with Fe_3O_4 content of 15 wt% as a function of exposure time within 50 s. At first 10 s, the specimen was heated, and did not exhibit the shape recovery. As the continuous procedure of magnetic fields, the recovery behaviors were triggered and the recovery ratio increased gradually. The recovery process finished at 50 s, and the ultimate recovery ratio was 87.1%. Figure 7(f) shows the recovery ratio of the composite film with Fe_3O_4 content of 15 wt% after five times of consecutive shape recovery and refixation process. The recovery ratio decreased from 88.9% to 72.5%, after five shape memory round processes. Afterwards, the recovery ratio kept stable of around 72%, indicating the reproducibility of shape memory behaviors.

Due to the excellent magnetic-triggered shape memory abilities of PAEK/Fe_3O_4 composites, we chosen the 15 wt% Fe_3O_4/PAEK composite to fabricate the magnetic responsive actuators and self-morphing structures, shown in figure 8. Figure 8(a) exhibited a kind of smart 'ball launcher'. Initially, the horizontal sample with the two layers of composite were heated up to the T_g (T_g + 10 °C) and fixed into the 'launcher' shape by the external force. Then, the splints of the two sides were opened and a ball was clamped in the launcher. Finally, while imposed with the external magnetic field, the opened splints gradually 'closed' to push out the ball, due to the magnetic-triggered shape recovery effect. Thus, the

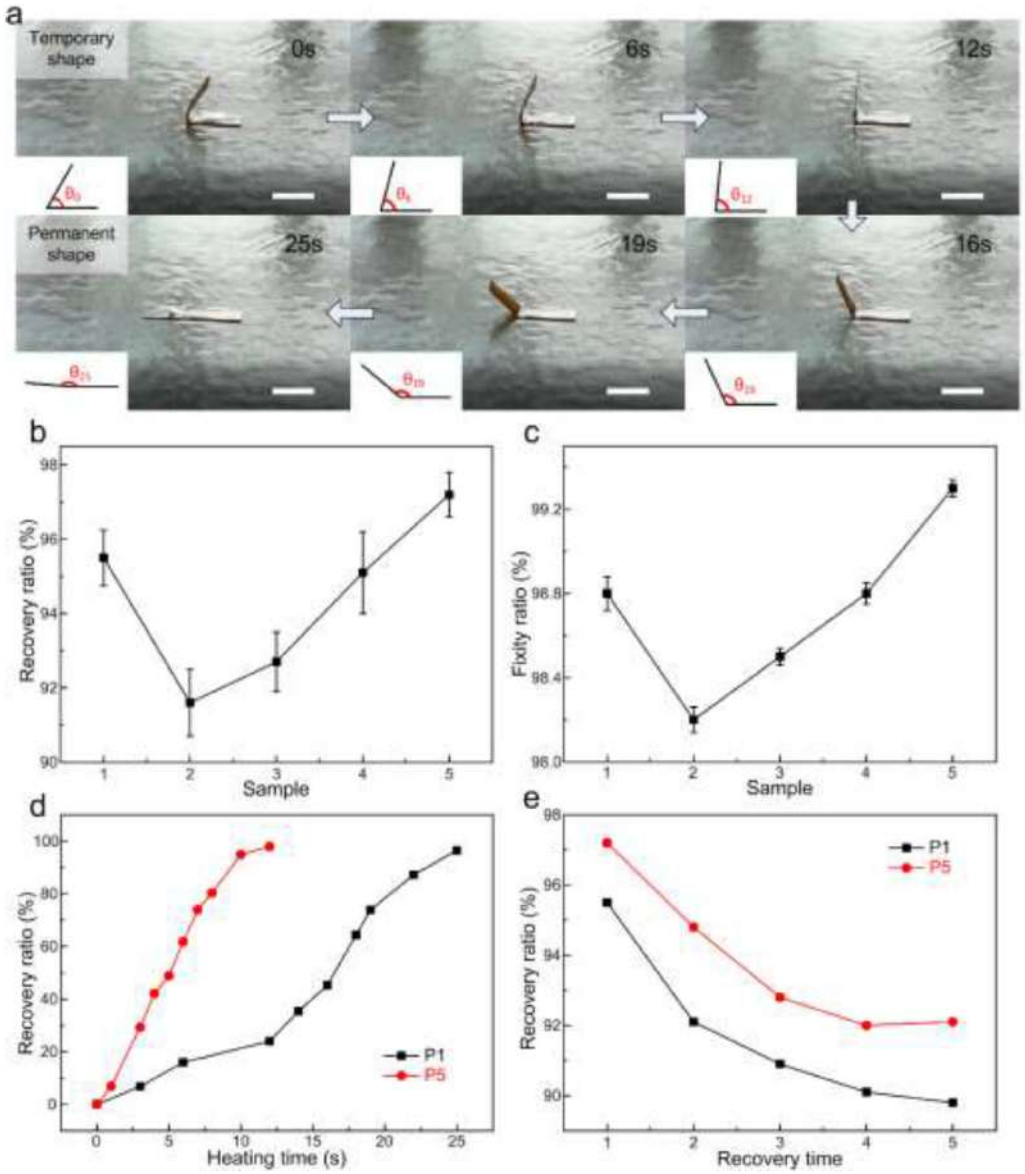

Figure 6. Heat-actuated shape memory behaviors of prepared PAEKs films: (a) the whole shape recovery process of P1 film at 131 °C (T_g + 10 °C); (b) shape recovery ratio; (c) shape fixity ratio; (d) recovery ratio of P1 and P5 as a function of heating time; (e) recovery ratio of P1 and P5 after five times of consecutive shape recovery process (scale bars of 1 cm).

ball could be launched which controlled by the external magnetic field. Figure 8(b) shows the diverse magnetic-triggered self-morphing structures, including smart 'flower' and 'plane'. For 'flower', initially, the four petals were opened, which was the original shape. Then, the temperature was increased up to T_g (T_g + 10 °C) and the petals were closed by external force to fabricate the temporary 'bud' shape. Afterwards, the closed petals could be opened again upon the magnetic field, and the whole 'bud' bloomed. As for 'plane', the wings were closed (horizontal shape) at initial. Then, the temperature was heated up to T_g (T_g + 10 °C), and the wings were opened (vertical shape) by external force. Finally, the wings were 'closed' while imposed with the applied magnetic field. These shape memory PAEK/Fe_3O_4 composite actuators exhibited the wide utilization potential in fields of smart actuators, flexible robotics, and deformable structures.

3.4. SAXS analysis of structural variation

Both heat- and magnetic-actuated shape recovery behaviors occurred at the internal temperature above T_g, even though they were realized by directed heating or magnetocaloric effect, respectively. Therefore, it was worthy to investigate the change of internal structures and orientation of molecular chains during the heating process. Heating SAXS patterns of P1 (from 25 °C to 130 °C) was performed for the investigation, as depicted in figure 9. In figure 9(a), P1 exhibited round scattered signals (observed in figure 2(a)) at 25 °C. When the temperature was up to 45 °C, the slight oblate scattered signals appeared, and the intensity became stronger. At the temperature of 80 °C, the oblate scattered signals were mostly clear. Once the temperature was 95 °C, scattering fringes similar to shish crystalline occurred at the

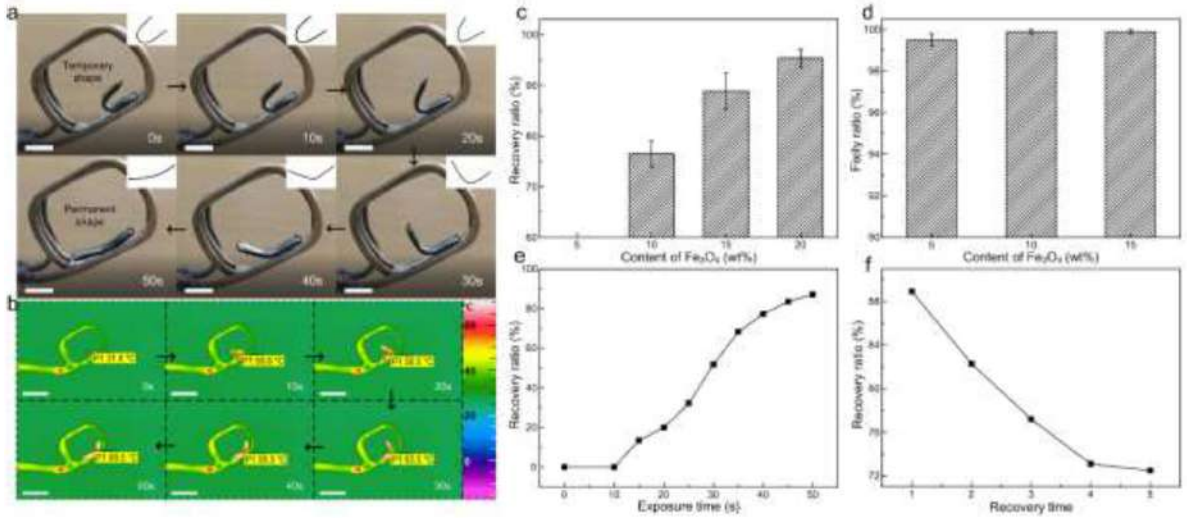

Figure 7. Non-contact magnetic-triggered shape memory behaviors of prepared PAEK/Fe_3O_4 composite films with different content of Fe_3O_4 (5, 10, 15, and 20 wt%): (a) the whole shape recovery process of the composite film with 15 wt% content of Fe_3O_4; (b) thermal infrared images during the shape recovery process; (c) recovery ratio; (d) fixity ratio; (e) recovery ratio as a function of exposure time; (f) recovery ratio after five times of consecutive shape recovery process (untagged scale bars of 1 cm).

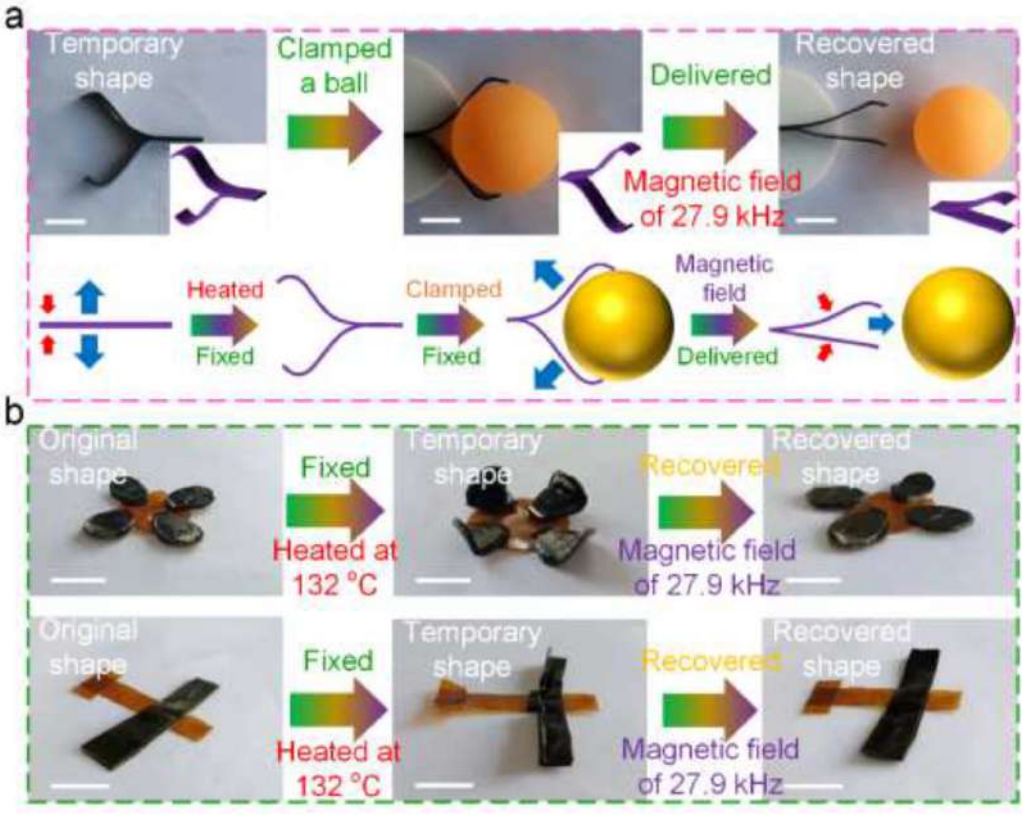

Figure 8. Shape memory 15 wt% Fe_3O_4/PAEK composites: (a) actuators of ball launcher; (b) self-morphing structures of smart 'flower' and 'plane' (scale bars of 1 cm).

vertical direction, and the whole scattered signals presented rhombic. The rhombic scattered signals became stronger at the temperature of 105 °C. Afterwards, while the temperature increased over 115 °C, the horizontal oblate scattered fringes became tilted. Finally, when the temperature reached up to 130 °C, the rhombic scattered signals became weak owing to the almost finish of glass-rubber state transition. In the heating process, we could obtain that in stage I (25 °C–45 °C), there was not orientation of molecular chains. In stage II (45 °C–95 °C), the molecular chains began to orientate. In stage III (95 °C–125 °C), as the transition of glass-rubber state, the phase transition occurred, and the orientation of

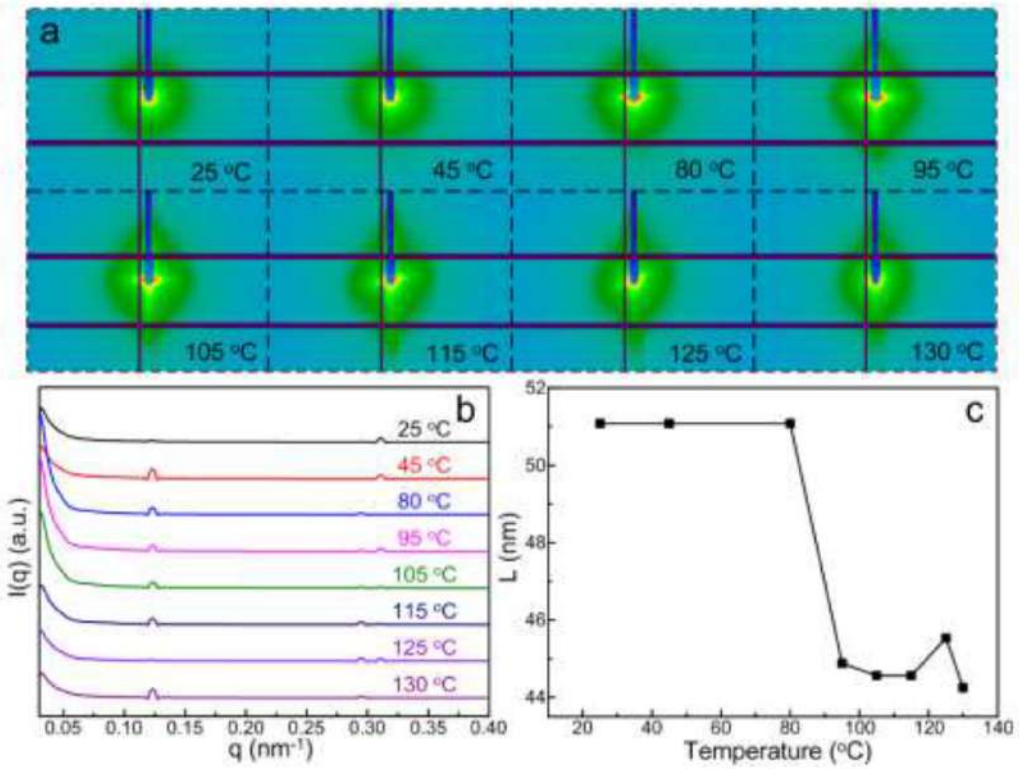

Figure 9. (a) Two-dimensional SAXS patterns; (b) 1D integral curves; and (c) the long period and q_{max} as a function of temperature during the heating process (from 25 °C to 130 °C).

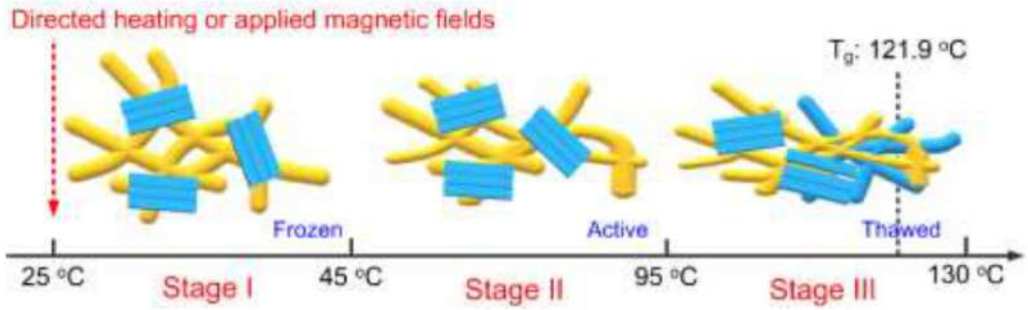

Figure 10. Schematic representation of the internal structures of PAEK polymers during the heating process (Molecular chains in amorphous regions were signed in yellow, and which of crystalline were signed in blue.).

molecular chains changed. As the completion of the whole transition phase (at 130 °C), the orientation of molecular chains weakened. In figure 9(b), as the increasing of temperature, the peak shifted to the higher q value. In figure 9(c), the long period maintained constant until the temperature was up to 80 °C. Afterwards, the long period decreased as the increasing of temperature. The phase state transformation from glass state to rubber state decreased the distance among the internal crystalline lamellae, resulting in the decreasing long period.

Through the analysis of the varying SAXS patterns during heating, it was found that the molecular chains of polymers during the whole heating process included three main stages, as depicted in figure 10 (P1 with T_g of 121.9 °C for example). In stage I, molecular chains of polymers were frozen, which were too difficult to orientate spontaneously. Polymers exhibited stationary glass state, contributing to shape fixity. With the continuous heating, the 'frozen' molecular chains became relatively active in the second stage. Though they still were not free to move, the orientation of molecular chains had occurred. When the temperature reached up around the T_g, the molecular chains began to melt to allow movement and orientation for achievement of shape recovery in the third stage. PAEKs then exhibited rubber state, and the shape recovery behaviors were finished during this stage. Whatever directed heating or magnetocaloric effect, the sufficient heat power endowed the molecular chains motional ability, promoting the occurrence of shape recovery.

4. Conclusions

In summary, we synthesized a series of shape memory PAEKs with different proportions of bisphenol monomers via the condensation polymerization. With the varying proportions of bisphenol monomers, the tuning of regularity and flexibility of main chains was achieved, and as a result, the alternating rigid-flexible main chains determined the transition temperature and shape memory behaviors. Synthesized PAEKs possessed wide T_g range from 121.9 °C to 159.3 °C, which increased gradually with the decreasing of side amino groups. Static SAXS patterns exhibited that the similar distribution of internal crystalline lamellae among prepared PAEKs. As the decreasing of side amino groups, the tensile strength and Young's modulus decreased gradually, concerning with the weakened stiffness of main chains. The combination of SAXS and tensile process revealed that the orientation of molecular chains occurred along with the applied force. Continuing to apply force, the microcracks occurred at the vertical direction to the applied force. The gathering of microcracks resulted in the fracture of specimens. Meanwhile, the distance between the internal crystalline lamellae slightly increased by the applied force, which was well indicated by the increasing long period value.

The fabricated shape memory PAEK films exhibited excellent fixity ratio (over 98%) and high recovery ratio (over 91%). As the decreasing of side amino groups, the recovery ratio and fixity ratio increased gradually. The regularity of molecular chains was conducive to the shape recovery. In addition, PAEK films possessed the great reproducibility of shape memory behaviors, which maintained high recovery ratio after the five times of consecutive shape memory processes. Non-contact actuated shape memory behaviors were achieved through the integration of magnetic Fe_3O_4 particles into PAEK matrix. As the increasing of Fe_3O_4 content, the magnetic-actuated recovery ratio increased gradually. Furthermore, based on the magnetic-triggered PAEK/Fe_3O_4 composites, we fabricated the smart magnetic-triggered actuators and self-morphing structures. The smart 'ball launcher' could launch the ball upon the applied magnetic field. Besides, the deformation actions of smart 'flower' and 'plane' could be controlled by the applied magnetic field. In the shape recovery process, the orientation of molecular chains occurred with the increasing of temperature, and resulted in glass-rubber transition state. Undoubtedly, the internal structures transformed along with the phase transition. The transition of internal molecular chains and crystalline lamellae during the heating process (directed heating or magnetocaloric effect) contributed to the shape recovery. This paper has offered a facile approach for the fabrication of shape memory composite actuators with desirable non-contact actuated SME, which could be used in the universal fields of aerospace, engineering industry, and smart devices.

Data availability statement

All data that support the findings of this study are included within the article (and any supplementary files).

Acknowledgments

This work is supported by the National Natural Science Foundation of China (Grant No. 11632005), and the Heilongjiang Touyan Innovation Team Program. The SAXS experiments were carried out at beamline BL19U2 of Shanghai Synchrotron Radiation Facility (SSRF).

Conflict of interest

The authors declare that they have no conflict of interest.

ORCID iDs

Yanju Liu https://orcid.org/0000-0001-8269-1594
Jinsong Leng https://orcid.org/0000-0001-5098-9871

References

[1] Melly S K, Liu L W, Liu Y J and Leng J S 2020 Active composites based on shape memory polymers: overview, fabrication methods, applications, and future prospects *J. Mater. Sci.* **55** 10975–1051
[2] Huang X Z, Zhang F H, Liu Y J and Leng J S 2020 Active and deformable organic electronic devices based on conductive shape memory polyimide *ACS Appl. Mater. Interface* **12** 23236–43
[3] Li X, Liu W K, Li Y M, Lan W L, Zhao D G and Wu H C 2020 Mechanically robust enzymatically degradable shape memory polyurethane urea with a rapid recovery response induced by NIR *J. Mater. Chem.* B **8** 5117
[4] Yan C, Yang Q X and Li G Q 2020 A phenomenological constitutive model for semicrystalline two-way shape memory polymers *Int. J. Mech. Sci.* **177** 105552
[5] Khoury L R, Slawinski M, Collison D R and Popa I 2020 Cation-induced shape programming and morphing in protein-based hydrogels *Sci. Adv.* **6** eaba6112
[6] Herbert K M, Getty P T, Dolinski N D, Hertzog J E, de Jong D, Lettow J H, Romulus J, Onorato J W, Foster E M and Rowan S J 2020 Dynamic reaction-induced phase separation in tunable, adaptive covalent networks *Chem. Sci.* **11** 5028
[7] Wang Y K, Chen Z H, Niu J H, Shi Y, Zhao J P, Ye J J and Tian W C 2020 Electrically responsive shape memory composites using silver plated chopped carbon fiber *Front. Chem.* **8** 322
[8] Xing S T, Wang P P, Liu S Q, Xu Y H, Zheng R M, Deng Z F, Peng Z F, Li J Y, Wu Y Y and Liu L 2020 A shape-memory soft actuator integrated with reversible electric/moisture actuating and strain sensing *Compos. Sci. Technol.* **193** 108133
[9] Wong T W, Behl M, Yusoff N I S M, Li T F, Wahit M U, Ismail A F, Zhao Q and Lendlein A 2020 Bio-based composites from plant based precursors and hydroxyapatite with shape-memory capability *Compos. Sci. Technol.* **194** 108138
[10] Chen S J, Yang S X, Li Z Y, Xu S W, Yuan H M, Chen S G and Ge Z C 2015 Electroactive two-way shape memory polymer laminates *Polym. Compos.* **36** 439–44
[11] Wang S Q, Kaneko D, Okajima M, Yasaki K, Tateyama S and Kaneko T 2013 Hyperbranched polycoumarates with photofunctional multiple shape memory *Angew. Chem., Int. Ed.* **52** 11143–8

[12] Peng W J *et al* 2020 Light-coded digital crystallinity patterns toward bioinspired 4D transformation of shape-memory polymers *Adv. Funct. Mater.* **30** 2000522
[13] Du W N, Jin Y, Shi L J, Shen Y C, Lai S Q and Zhou Y T 2020 NIR-light-induced thermoset shape memory polyurethane composites with self-healing and recyclable functionalities *Composites* B **195** 108092
[14] Zhou C H, Ni Y R, Liu W T, Tan B, Yao M C, Fang L, Lu C H and Xu Z Z 2020 Near-infrared light-induced sequential shape recovery and separation of assembled temperature memory polymer microparticles *Macromol. Rapid Commun.* **41** 2000043
[15] Banikazemi S, Rezaei M, Rezaei P, Babaie A and Eyvazzadeh-Kalajahi A 2020 Preparation of electrospun shape memory polyurethane fibers in optimized electrospinning conditions via response surface methodology *Polym. Adv. Technol.* **31** 2199–208
[16] Yan K, Xu F Y, Li S H, Li Y Y, Chen Y L and Wang D 2020 Ice-templating of chitosan/agarose porous composite hydrogel with adjustable water-sensitive shape memory property and multi-staged degradation performance *Colloid Surf.* B **190** 110907
[17] Roy P and Sailaja R R N 2015 Mechanical, thermal and bio-compatibility studies of PAEK-hydroxyapatite nanocomposites *J. Mech. Behav. Biomed.* **49** 1–11
[18] Wang W T, Wang F, Zhang C, Wang Z K, Tang J N, Zeng X R and Wan X J 2020 Robust, reprocessable, and reconfigurable cellulose-based multiple shape memory polymer enabled by dynamic metal−ligand bonds *ACS Appl. Mater. Interfaces* **12** 25233–42
[19] Wu M Y, Sukyai P, Lv D, Zhang F, Wang P D, Liu C and Li B 2020 Water and humidity-induced shape memory cellulose nanopaper with quick response, excellent wet strength and folding resistance *Chem. Eng. J.* **392** 123673
[20] Fer G L and Becker M L 2020 4D printing of resorbable complex shape-memory poly(propylene fumarate) star scaffolds *ACS Appl. Mater. Interfaces* **12** 22444–52
[21] Chen Z Y, Wang Z, Hou L, Wang C M, Du X M, Liu C, Liu W C, Li H Q and Xu J M 2019 A simple self-regulating permeability and selectivity of poly (arylene ether ketone) with amino groups for gas separation membrane *J. Polym. Res.* **26** 267
[22] Li H, Luo D W, He J L, Lin F, Wang H, Yu L, Liu W and Li J 2020 Crystalline Al_2O_3 modified porous poly(aryl ether ketone) (PAEK) composite separators for high performance lithium-ion batteries via an electrospinning technique *CrystEngComm* **22** 1577–85
[23] Du X M, Wang Z, Liu W C, Xu J M, Chen Z Y and Wang C M 2018 Imidazolium-functionalized poly (arylene ether ketone) cross-linked anion exchange membranes *J. Membr. Sci.* **266** 205–12
[24] Gu Y Y, Ru C Y, Zhao Z, Chao D M and Liu X C 2020 Performance enhancement of shape memory poly(aryl ether ketone) via photodimerization of pendant anthracene units *Eur. Polym. J.* **123** 109413
[25] Lu Y, Pan X T, Li N, Hu Z X and Chen S W 2020 Improved performance of quaternized poly(arylene ether ketone)s/graphitic carbon nitride nanosheets composite anion exchange membrane for fuel cell applications *Appl. Surf. Sci.* **503** 144071
[26] Liao J B, Wang J L, Liu Z and Ye Z B 2019 Polar benzimidazole-containing (sulfonated) poly(arylene ether ketone)s as bifunctional binders for lithium-sulfur battery cathodes with high sulfur loadings *ACS Appl. Energ. Mater.* **2** 6732–40
[27] Mu S L, Zhang Y Q, Zhou J J, Wang B X and Wang Z K 2020 Recyclable and mechanically robust palm oil-derived epoxy resins with reconfigurable shape-memory properties *ACS Sustain. Chem. Eng.* **8** 5296–304
[28] Le H T, Wang C G and Goto A 2020 Solid-phase radical polymerization of halogen-bond-based crystals and applications to pre-shaped polymer materials *Angew. Chem., Int. Ed.* **59** 9360–4
[29] Herath M, Epaarachchi J, Islam M, Zhang F H, Leng J S, Fang L, Yan C, Peng G D and Schade W 2020 Remote actuation of light activated shape memory polymers via D-shaped optical fibres *Smart Mater. Struct.* **29** 047001
[30] Gupta R K, Hashmi S A R, Verma S, Naik A and Nair P 2020 Recovery stress and storage modulus of microwave-induced graphene-reinforced thermoresponsive shape memory polyurethane nanocomposites *J. Mater. Eng. Perform.* **29** 205–14
[31] Gao Y L, Zhu G M, Xu S G, Ma T T and Nie J 2018 Biodegradable magnetic-sensitive shape memory poly(ε-caprolactone)/Fe_3O_4 nanocomposites *J. Appl. Polym. Sci.* **135** 45652
[32] Liu Y Q, Xu K G, Chang Q, Darabi M A, Lin B J, Zhong W and Xing M 2016 Highly flexible and resilient elastin hybrid cryogels with shape memory, injectability, conductivity, and magnetic responsive properties *Adv. Mater.* **28** 7758–67
[33] Meiorin C, Actis D G, Montoro F E, Londono O M, Aranguren M I, Muraca D, Zelis P M, Knobel M and Mosiewicki M A 2018 Magnetic remote activation of shape recovery in nanocomposites based on tung oil and styrene *Phys. Status Solidi* A **215** 1800311
[34] Razzaq M Y, Behl M, Nochel U and Lendlein A 2014 Magnetically controlled shape-memory effects of hybrid nanocomposites from oligo(u-pentadecalactone) and covalently integrated magnetite nanoparticles *Polymer* **55** 5953–60
[35] Wang Y K, Ye J J and Tian W C 2016 Shape memory polymer composites of poly(styrene-b-butadiene-b-styrene) copolymer/liner low density polyethylene/Fe_3O_4 nanoparticles for remote activation *Appl. Sci.* **6** 333
[36] Wang L Y, Yang Y, Chen Y H, Majidi C, Iida F, Askounis E and Pei Q B 2018 Controllable and reversible tuning of material rigidity for robot applications *Mater. Today* **21** 563–76
[37] Chatterjee R, Singh A, Kumar A G, Voit B and Banerjee S 2020 Synthesis and characterization of star-shaped sulfonated new poly(ether triazole)s: proton exchange membrane properties *Eur. Polym. J.* **123** 109443
[38] Yang S, Ahn Y and Kim D 2017 Poly(arylene ether ketone) proton exchange membranes grafted with long aliphatic pendant sulfonated groups for vanadium redox flow batteries *J. Mater. Chem.* A **5** 2261–70